Published in "Advanced Engineering Materials 11(8): 659 - 666, 2009"
which should be cited to refer to this work.

Activation Mechanism and Infiltration Kinetic for Pressureless Melt Infiltration of Ti Activated Al_2O_3 Preforms by High Melting Alloy**

By *Srdan Vasić,* Bernard Grobéty, Jakob Kuebler* and *Thomas Graule*

Metal matrix composites (MMC) represent a class of materials of broad technological and commercial significance designed for applications where the contrasting material properties of both metals and ceramics are needed.[1] MMC combine the high strength and wear resistance of ceramics with the ductility as well as the thermal and electrical conductivity of metals. The ceramic phase within the metal matrix guarantees a failure-tolerant behavior and low thermal expansion.[2] Many fabrication routes have been described in previous studies,[3] the most important ones are pressureless and pressure assisted metal melt infiltration techniques as well as powder metallurgical methods. The choice of a suitable manufacturing route is conditioned by cost factors, form flexibility and production temperature,[3,4] For certain applications in the food, pharmaceutical and automotive industry, the required properties are best met by composites made of alumina (Al_2O_3) and high-melting Fe-based alloys (>1400 °C) such as X3CrNi13-4.[5–9] Pressureless infiltration would be the manufacturing route of choice for many of these applications, but the alumina-steel system lacks an important prerequisite, that makes infiltration without pressure possible: Oxide ceramics in general, due to their ionic character, show bad wettability by metal melts. The equilibrium contact angle θ_Y, which depends on the surface tensions of the phases involved, is given by Young's equation [10–12] (Eq. 1):

$$\cos\theta_Y = \frac{\sigma_{SV}\,\sigma_{SL}}{\sigma_{LV}} \tag{1}$$

[*] *Dr. S. Vasić, Prof. B. Grobéty*
Technical Mineralogy Group, Institute of Mineralogy and Petrography, University of Fribourg
Pérolles, Ch. du Musée 6, CH-1700 Fribourg, Switzerland
E-mail: srdan.vasic@unifr.ch
Dr. S. Vasić, J. Kuebler, Prof. T. Graule
Empa, Swiss Federal Laboratories for Materials Testing and Research, Laboratory for High Performance Ceramics
Ueberlandstrasse 129, CH-8600 Duebendorf
E-mail: jakob.kuebler@empa.ch; thomas.graule@empa.ch

[**] *The authors would like to thank Jean-Paul Bourqui (University of Fribourg) for the excellent preparation of the SEM samples and Christoph Neurrurer (University of Fribourg) for the fabrication of in situ activated alloys.*

and is in general well over 90° for such systems.[13–16] It is therefore not surprising that steel melts do not wet alumina surfaces.

Pressure assisted infiltration and previous activation of the metal and/or the ceramic preform by incorporating reactive metals like titanium (Ti) are the two methods at disposal to circumvent the wettability problem.[2,7] Moreover, it was shown that a pressure drop within preforms, caused by the reaction of reactive metals such as e.g. Ni, Ti or Al and thus generation of a vacuum atmosphere is favorable for successful infiltration.[17] Applying pressure to the melt allows overcoming the negative capillary forces, but the pressurizing systems are technically demanding. The addition of a reactive element such as Ti enhances the infiltration performance either by lowering the surface tension of the metal melt and/or by the reactive modification of the ceramic surface.[18] It is well known that the addition of Ti to brazing solders for joining ceramic components lowers the contact angle of the metal melt with alumina due to the formation of a reactive layer.[19,20] Addition of titanium to steel melts lowers the surface tension, although there is a large spread in the data which are due to the presence or absence of surface active species in the gas phase. The formation of a TiO_x reactive layer, and also modification of fluid flow and active metal adsorption are additional mechanisms that have been postulated to enhance wettability.[21,22] The activator may be prealloyed into the metal or dispersed into the porous ceramic preform, which guarantees a gradual dissolution of the activator into the infiltration melt.[23] This technique was successfully applied to infiltrate porous SiC and AlN preforms with bronze and Fe-base alloys.[24] The Ti in this case forms a reactive, wettable TiC layer on the surface of the carbide grains. Activated alumina preforms were infiltrated by Fe- and Ni-base alloys, but in this case the activation mechanism has not been demonstrated.[5–9]

Pressureless infiltration in wettable systems is mainly driven by capillary forces and gravity. Capillary phenomena are increasingly important for systems with pore channels smaller than 1 μm, whereas gravity is the main force for the filling of pores larger than 10 μm in diameter.[25] The rate of capillary flow is described by Darcy's law, which indicates a parabolic time dependence of infiltration depth[26] (Eq. 2):

$$x = \left(\frac{2KP}{\eta}\right)^{1/2} t^{1/2} \tag{2}$$

Table 1. Next nearest titanium interparticle distances d_i for activation contents i, average pore diameter D_p and total porosity π of the preforms determined by X-ray tomography and mercury intrusion porosimetry by Vasic et al.(2007) [34].

d_1 [μm]		d_3 [μm]	d_5 [μm]	d_{10} [μm]	d_{20} [μm]	D_p [μm]	π[%]
A100T40A20T40	130 139	83 104	70 84	64 71	53 59	~25 ~7	~45 ~40
A100T200	–	292	–	232	171	~25	~40
A20T200	–	350	–	258	173	~7	~45

Table 2. Nominal average composition and melting temperatures of the investigated alloy.

Notation	W. Nr.	Alloying elements in wt% Fe	Cr	Mo	Ni	C	Other elements
X3CrNiMo13-4	1.4313	80.2	13	0.5	4	0.1	Mn: 0.5; Si: 0.5; S: 0.015

where η describes the viscosity, K the permeability and P the capillary pressure. The above equation is the asymptotic solution corresponding to the short time solution to the Newton dynamics equation describing the rise in a capillary tube.[27] Parabolic time dependence for the infiltration of metallic melts to ceramic porous bodies have been observed e.g., for the systems TiC-AlNi[28] and SiC-AlSiMg.[29] Preliminary results from infiltration experiments of alumina preforms by Fe- and Ni-base alloys indicated not a parabolic but rather a linear time dependence of the infiltration rate.[30] Linear time dependence has been reported for infiltration systems such as SiC-CoSi[31] and AlN-Al.[32] Spreading of the liquid over the pore walls has been suggested as a rate limiting step. A wide range of spreading kinetics for liquid spreading on solids have been observed, most of which follow a power law e.g. show a $t^{1/n}$ dependency with n ranging from 1 to 50. Linear spreading kinetics (e.g. $n=1$) have been observed for several reactive metal melt–ceramic systems at high temperature such as Al melt on vitreous carbon[33] or CuAgTi melt on alumina.[34]

In this work we will focus on the pressureless melt infiltration Fe-based alloy into, Ti (titanium)-activated porous ceramic powder compact. The goal of the study is to analyze the infiltration kinetic and to understand the activation mechanism in this system.

Experimental

Materials and Setup for Infiltration Experiments

Porous alumina preforms were prepared with fine (A20) and coarse (A100) alumina powders mixed with different amounts of either fine (T40) or coarse (T200) titanium activator. Pressed pellets (~6 mm high, 14 mm diameter, 65 MPa) of powder mixtures A100T40-i and A20T40-i with $i=1$, 3, 5, 10, and 20 wt% of titanium activator (based on the Al_2O_3/Ti powder mixtures) and A100T200-i and A20T200-i with $i=3$, 5, and 20 wt% Ti were fabricated. Average pore diameter and porosity of the powder compacts were analyzed by mercury intrusion porosimetry, helium pycnometry, and mercury buoyancy methods. The 3D microstructure, the spatial distribution of the titanium particle, and the inter-particle distances were obtained from X-ray tomography measurements (Table 1).

A detailed description of the preparation and characterization of the preforms can be found in ref. [35]. The set of experiments was made with a X3CrNiMo13-4 steel (Böhler AG; Switzerland, Walisellen). The alloy composition is shortly summarized in Table 2.

The steel samples were cut in small cubes (~1 cm^3). Before the samples were placed on top of a preform, the oxide layer was removed by grinding and the surfaces cleaned with acetone in an ultrasonic bath. The amount of metal used corresponds to about twice the pore volume of the preforms. For the infiltration experiments the preform-steel cube couples were placed in alumina crucibles (Fig. 1). The crucible walls were covered with alumina powder to prevent sintering between sample and crucible. The infiltration experiments were made in a conventional vacuum furnace with molybdenum lining (Super VII, Centorr Vacuum Industries, Summerville MA, USA). Temperature was increased with a heating

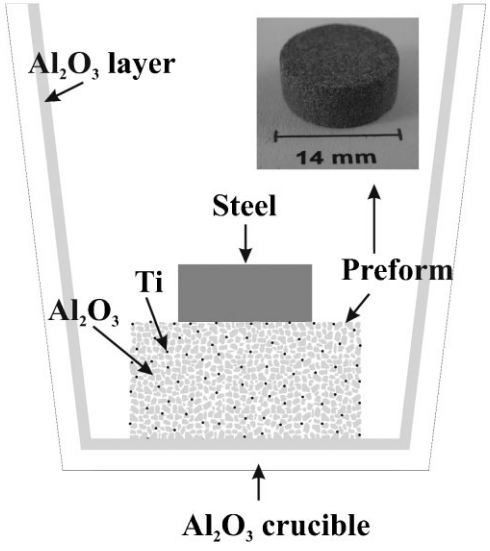

Fig. 1. Schematic infiltration setup.

rate 5 °C min^{-1} up to 1600 °C, e.g. ~65 °C above the melting temperature of X3CrNiMo13-4. The experiments were carried out with dwell times at 1600 °C of 1, 10, 20, 30, and 120 min. The time span the samples were above the melting temperature corresponds to the dwell time plus 2×13 min, thus 27, 36, 56, and 146 min. All experiments were conducted in a vacuum of 2.5×10^{-4} mbar.

Wetting Experiments

Simple sessile drop experiments were performed, in order to test the influence of titanium on the surface tension of X3CrNi13-4 alloy. Pieces of steel containing different concentration of titanium (8, 16, and 22 wt% T40, based on the weight of the alloy piece) were placed on polycrystalline alumina substrates (AC Applied Ceramics, Schaan, Switzerland) with a surface roughness of ~0.4 μm and heated in the same vacuum furnace, in which the infiltration experiments were performed (heating rate of 5 °C min^{-1}, dwell time: 30 min at 1600 °C, vacuum: 2.5×10^{-4} mbar). Contact angles were determined after cooling. The X3CrNi13-4 –Ti alloys were synthesized in an induction furnace. Different amounts of titanium were filled in holes drilled into steel cubes. The holes were closed with steel threads and the cubes heated under vacuum (1×10^{-5} mbar) for 15 min above the melting point of the system. The surface oxide layer was removed by grinding. SEM and EDS measurement of the Ti alloyed X3CrNiMo13-4 steels showed that they consisted of a single homogeneous phase. Additionally a piece of X3CrNi13-4 steel was placed on a substrate coated with a 10 μm Ti layer. As reference, a sessile drop experiment with pure X3CrNi13-4 was made.

Characterization Methods

After removing the infiltrated samples from the crucibles, polished, resin impregnated cross-sections were prepared for characterization by optical microscopy (Zeiss Axiovert 100 A, Jena, Germany) and scanning electron microscopy (SEM; FEI XL Sirion FEG, Eindhoven, Netherlands equipped with an EDAX energy dispersive system). It was difficult to avoid the pull-out of loosely bound alumina particles in uninfiltrated areas of the sample. The depth of the infiltration front (definition see below) was rarely constant over the entire section; therefore, the average of 14 equidistant depth measurements were taken for the evalutaion of the infiltration kinetics (Fig. 2). The gravimetric determination of the infiltrated volume fraction as measure of the infiltration progress (see e.g. Pan et al., 1999) was not a suitable method for reasons, which will become clear later on. The steel distribution in one of the partially infiltrated samples (A100T40-20) has been analyzed by X-ray tomography (experimental details s. Vasic et al., 2007 [35]).

Results

Wetting Experiments

Pure X3CrNiMo13-4 steel shows non-wetting behavior relative to the alumina substrate and the furnace atmosphere.

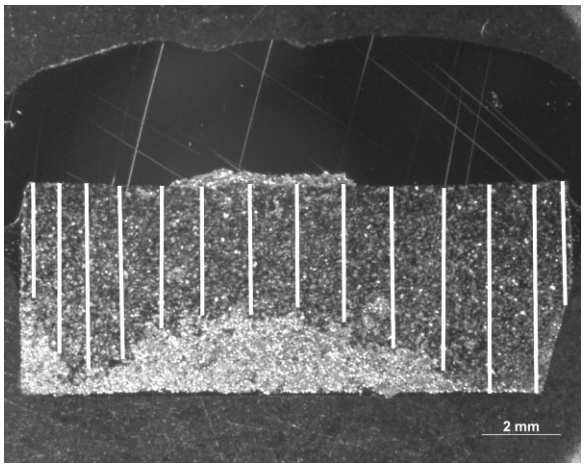

Fig. 2. 14 measurements (white lines) to determine the average infiltration depth h.

The measured contact angle after cooling the sample is 120°. The contact angle decreases almost linearly with increase in titanium concentration to an angle of 101° for 22 wt% Ti (Fig. 3a). The X3CrNiMo13-4 – Ti steel system, therefore, remains non-wetting for all Ti concentration up to 22 wt%Ti. (Fig. 3b). Infiltration experiments with the prealloyed steel were not successful.

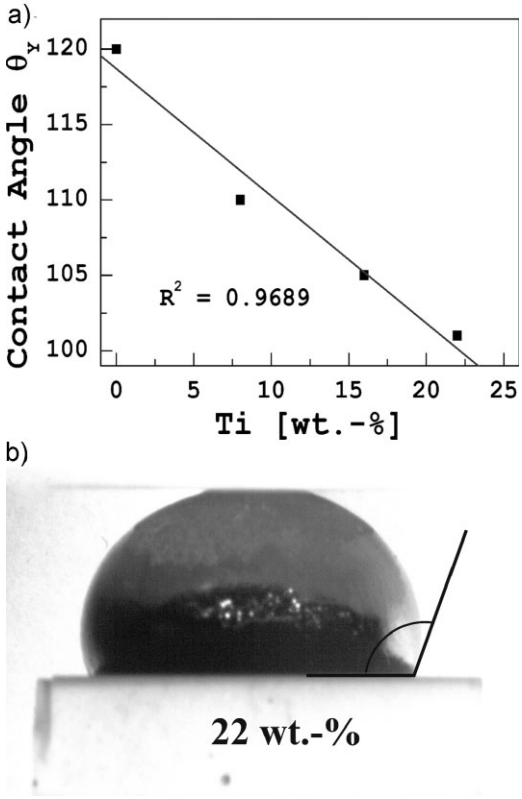

Fig. 3. (a) Measured contact angles for differently prealloyed Ti-X3CrNiMo13-4 steels; (b) light optical image used for the contact angle determination of the steel sample with 22 wt% Ti.

Infiltrated Samples

In most samples, two or three distinct zones could be distinguished along the infiltration direction. A fully (>95%) infiltrated zone (Z1) adjacent to the top of the preform, followed by a zone (Z2) (Fig. 4a), which appeared in the 2D sections to contain isolated Ti particles covered by a steel layer (''wetted islands'', WI, Fig. 4b) and a lower most zone (Z3) without any melt. The steel in Z2 filled about 20 to 30% of the pore volume of Z2 (estimation from optical microscopy images). In the following, the interface between Z1 and Z2 will be called infiltration front (IF, s. Fig. 4a). The presence of steel in Z2, e.g. beyond IF, precluded the use of gravimetric methods to determine the infiltration depth. In samples with either short dwell times and/or low activator concentrations and/or coarse activator powder (T200), the zone adjacent to the top of the samples was of type Z2. No fully infiltrated zone was present. In partially infiltrated samples, WI's were found up to 2 mm from the IF. The isolated nature of these ''islands'' was confirmed by X-ray tomography analyses of a partially infiltrated sample (Fig. 5). The reconstructed 3D images show that there is no connection between the WI's and Z1.

Samples with less than 5 wt% activator contained, regardless of the other experimental parameters (dwell time, alumina powder etc.), only Z2 and 3. A20T40 samples with 10 wt% activator contained only Z2 and Z3, samples with 20 wt% and long dwell times were partially infiltrated. A100T40 samples containing 5 wt% were partially infiltrated, samples with 10 and 20 wt% of Ti were fully infiltrated at long dwell times. Preforms with high enough activator content, but with an inhomogeneous distribution of the Ti particles contained non-infiltrated areas inside Z1 (Fig. 6). The Ti particle concentration in these areas was clearly lower than in the fully infiltrated neighborhood. When particles in Z2 are close enough (<ca. 20 μm), melt ''bridges'' (wetted bridges, WB) between particles were observed (Fig. 7a), which close to IF develop into fingerlike wetted trails connected with the fully infiltrated part of the preform (Fig. 7b).

The metal matrix composition was investigated on numerous samples infiltrated with X3CrNi13-4 steel (Table 3). The microstructure consists of a homogeneous phase with a Ti content that increases with increase in dwell time. The maximum Ti concentration in the matrix is ~2 wt%. A second titanium rich steel phase (ca. 10 wt%) can be found close to remains of Ti particle in samples with 120 min dwell

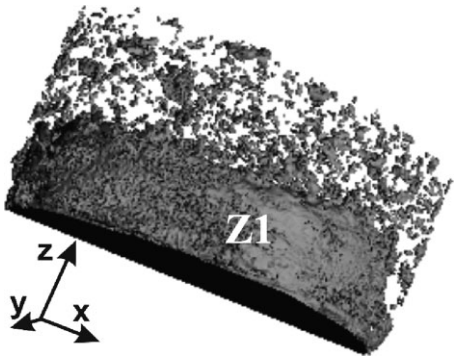

Fig. 5. X-ray tomography image of a partially infiltrated sample A100T40-20, dwell time 15 min (z represents the infiltration direction).

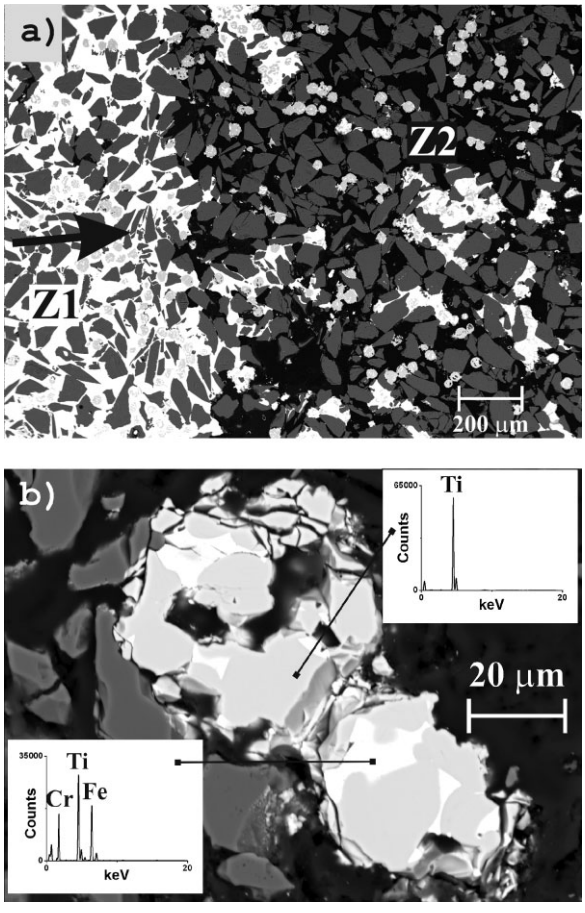

Fig. 4. (a) SEM image of a section across the infiltration front, defined as the boundary dividing Z1 and Z2. The black arrow shows the infiltration direction;(b) Partially wetted island in Z2 of sample A20T40-10 after a dwell time of 20 min. The insets show EDS measurement of the titanium particle and the steel cover.

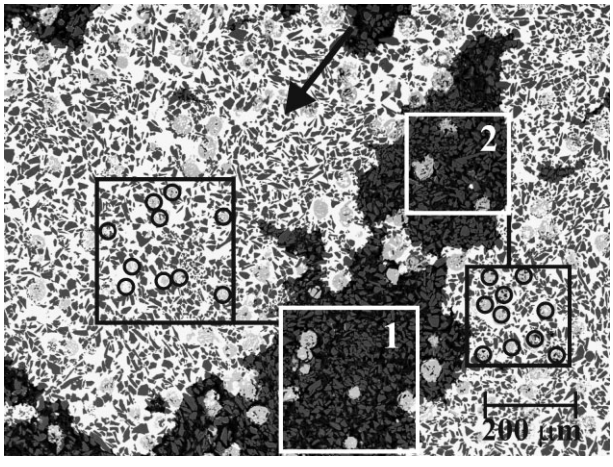

Fig. 6. Area in Z1 of sample A20T40-20 with inhomogeneous Ti particle distribution. Particle count in the not infiltrated areas 1 and 2 (white outlined): 3 and 7 Ti particles. Count in adjacent infiltrated areas of same size as the previous areas: 10 and 10 Ti particles. The black arrow shows the infiltration direction.

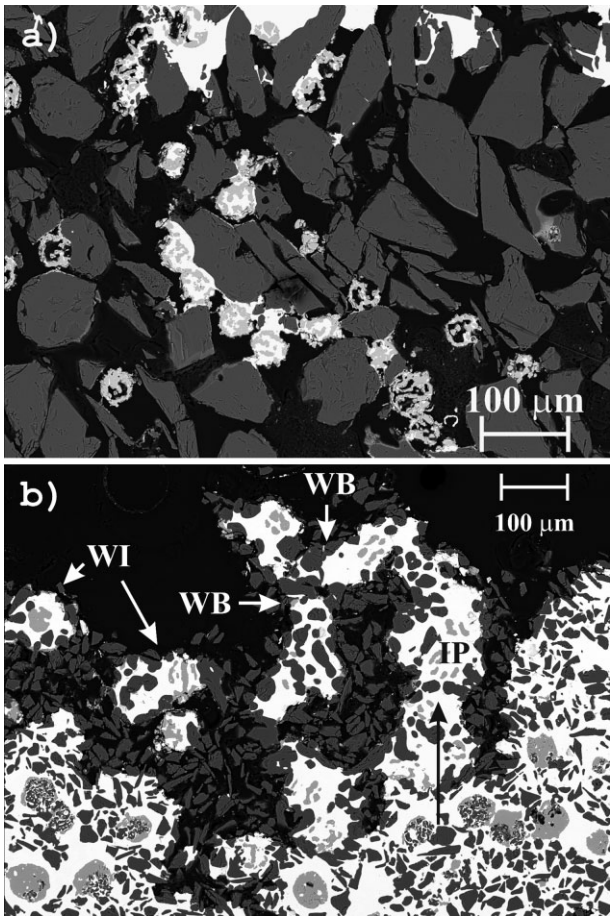

Fig. 7. (a) Wetted bridges in sample A100T40-10 after a dwell time of 1 min and (b) wetted trails connected to IF in sample A20T40-10 after a dwell time of 40 min.

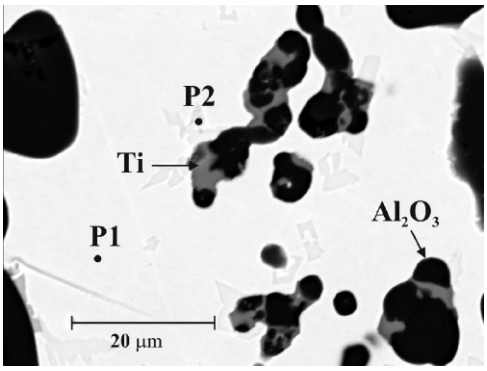

Fig. 8. In samples with long dwell times a second phase (P2) can be observed close to Ti particle remnants.

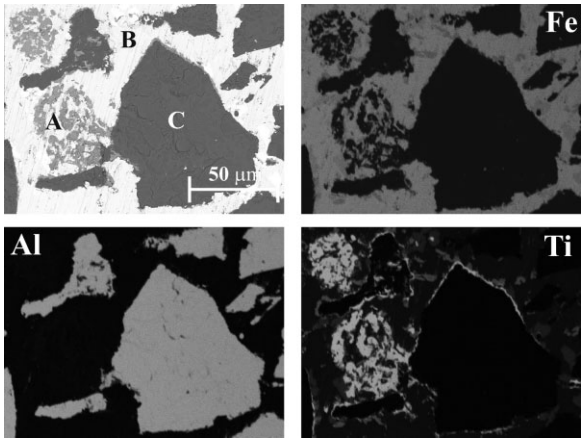

Fig. 9. EDS maps of A100T40-20 samples (dwell time 120 min; A: Ti; B: Alloy; C: Al2O3). The Ti map reveals titanium rich segregations along certain alumina grain boundaries.

time (Fig. 8). In the same samples, Ti rich alumina/steel segregations along alumina grain boundaries can be observed, but which are not continuous and not present everywhere (Fig. 9). The rounded morphology of the alumina grains in the same samples is clear signs of dissolution.

The infiltration rate was determined for four samples: A20T40-5, A100T40-20, 10, and 5 (Fig. 10a). For A20T40-5 and to a lesser degree A100T40-5, two regimes can be distinguished: one for short and one for longer infiltration times. The functional relationship for short dwell times is difficult to determine, it can be fit equally well with a linear and a $t^{1/n}$ relationship. For dwell times>20 min, the relationship is linear with a rate of 0.02 mm min^{-1}. For the two remaining samples, the shortest dwell times were already in the linear regime. The slopes in the linear regime of samples A20T40-5, A100T40-20, and −5 are equal, but the curves are displaced along the y-axis. The data points for sample A100T40-10 also show a linear relationship, but with a shallower slope than the other three samples. The penetration depths of the three A100T40-i samples increase linearly with activator content i (Fig. 10b).

Table 3. Steel compositions in samples as a function of dwell time and activation contents. ± Indications: spread in data.

Notation	Ti (wt%)	Cr (wt%)	Fe (wt%)	Ni (wt%)	t_d	Remarks
A20T40-20	2.13/±0.3	12.37/±0.5	82.13/±0.2	2.13/±0.3	120	1stPhase (P1)
A20T40-20	10.46/±3.0	9.47/±0.9	75.63/±2.7	4.44/±0.7	120	2ndPhase (P2)
A20T40-20	1.96/±0.5	12.31/±0.5	82.29/±0.5	3.44/±0.5	30	–
A100T40-5	1.46/±1.1	12.31/±1.1	82.69/±1.0	3.54/±1.0	30	–
A100T40-5	1.26/±0.1	12.39/±0.2	82.01/±0.1	4.35/±0.2	10	–

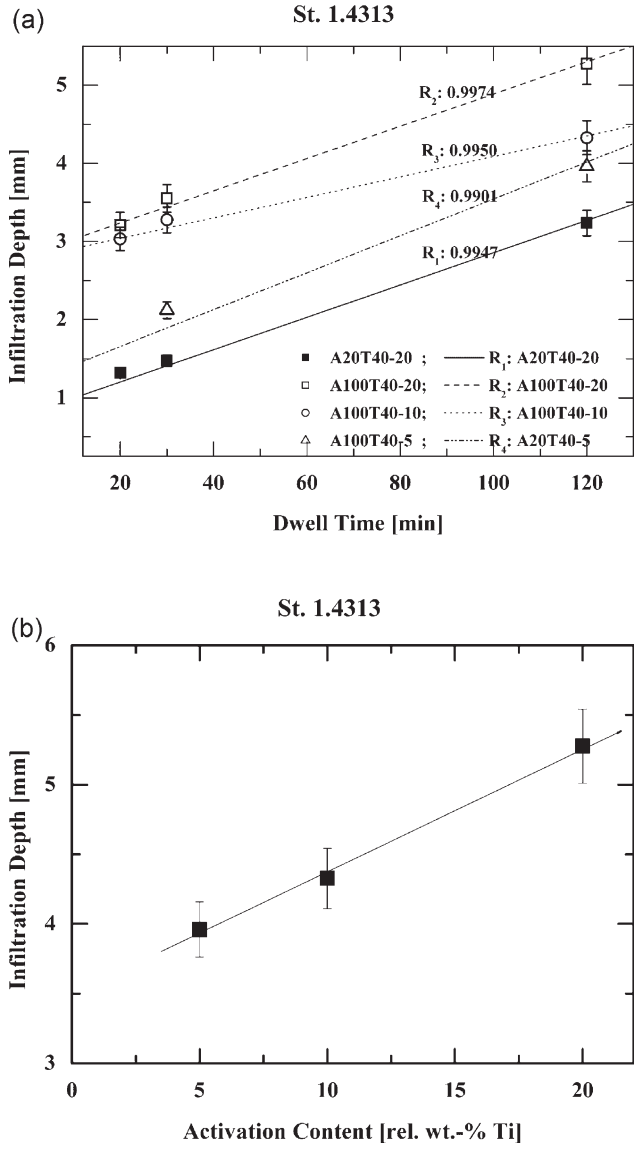

Fig. 10. (a) Infiltration depths as function of dwell time. The time span the samples were above the melting temperature of the steel is equal to the dwell time plus 2 × 13 min during heating and cooling between melt (~1535 °C) and dwell temperature (1600 °C). (b) Infiltration depths as function of activator content for A100T40 samples and 120 min dwell time.

Discussion

Activation Mechanism

The lowering of the contact angle and/or the modification of the alumina surface by the addition of the activator are the infiltration enhancement mechanisms found in previous activated infiltration experiments. There are a large number of data on the influence of alloying elements and gas phase species on the contact angle of Fe-base alloys with alumina. Reported contact angles at 1600 °C for pure iron melt on alumina at very low oxygen and sulfur activity vary between 121[36] and 147° [37] with most of the data clustering around values between 130 and 135°.[38–41] When increasing the oxygen activity, the contact angle decreases with time to values well below 90°. The increased wettability is due to the formation of hercynite ($FeAl_2O_4$) at the interface.[39] Adding small amounts of Ti (8 wt%) at low oxygen activity lowers the contact angle of iron melts to values around 90°, which remains constant when further increasing the content of Ti up to 22 wt%.[42] A much smaller decrease in contact angle (from 143 to 135°) with similar Ti concentrations has been observed for IF and LC steels.[43,44] The improved wettability is due to the segregation of Ti, which has a higher oxygen affinity. The enhanced absorption of oxygen will lower the surface tension of the alloy. Along the melt-alumina interface, the segregated Ti may form reactive layers consisting of titanium oxides e.g. Ti_2O_3 for samples with low Ti and TiO for higher Ti concentrations.[45] The alloy has a lower contact angle with these reactive layers than with the alumina surface. For Fe-16 wt% Cr alloy, which is close to the present steel composition, the contact angle with alumina at very low oxygen activity and a temperature of 1550 °C varies between 145 and 155°.[46]

These values are considerably larger than the contact angle observed for the present X3CrNi13-4 alloy. The higher temperature, higher oxygen partial pressures in the furnace atmosphere, and additional alloying elements Mo and Ni are the likely factors for the lower value. The observed contact angle decrease of Fe-Cr alloys on alumina with increasing Ti amount is in the line with the effect of Ti on pure iron and steel melts. The improvement is, however, not good enough for the alloy melt to become wetting. Reactive layers are only observed within Z1 of samples with long dwell times, but never at the contact between WI/alumina grains or close to IF. The reactive layers formed most likely after the infiltration front had passed. Improved wettability of the melt due to dissolution of the activator at the infiltration front and the formation of a reactive layer at the infiltration front, which are the mechanisms proposed in other activated infiltration systems,[23,24] may, therefore, be excluded for the present case.

Infiltration Kinetic

A possible key to understand the infiltration mechanism comes from the WI's observed in Z2 of partially infiltrated samples. The only possible explanation for the presence of the steel covering the Ti particles in Z2 is transport through the gas phase followed by condensates onto the Ti particle surface. They may, however, be an artifact produced during the cooling of the samples between the annealing and the solidification temperature of the steel, and, therefore, not been involved in the infiltration process. The vapor pressure of the alloy at 1600 °C is in the order of several Pa (pure iron: 8Pa; [47]).

This pressure is about two orders of magnitude larger than the furnace pressure. The steel vapor is, therefore, likely to permeate the entire pore volume of the sample. Assuming that the sample is not infiltrated and that all the steel vapor present in the pores at 1600 °C condensates onto Ti particles during cooling, the resulting condensation layer would only have a

thickness of about 2 nm, orders of magnitude less than observed in Z2.

A driving force that may lead to isothermal condensation is supersaturation. Supersaturation may occur because there is not one, but two different metallic phases present in the sample e.g. steel and Ti. The steel vapor will, close to the activator particles, mix with gaseous Ti in equilibrium with the solid titanium surface. The titanium vapor pressure at 1600 °C is 2.29×10^{-3} Pa for 1600 °C.[48] The gas mixing leads to a supersaturation relative to a specific Ti-bearing X3CrNi13-4 melt composition, which will, therefore, precipitate onto the activator surface. The remaining gas phase becomes depleted relative to the original steel vapor composition and a gradient will be established from the top surface of the sample, where the initial steel block is located, toward the interior of the preform. At a certain distance, which in our samples corresponds to the limit between Z2 and Z3, the gas phase becomes undersaturated relative to any titanium containing alloy melt and no condensation occurs anymore. Such a gradient is clearly visible along the side walls of certain preforms, where the original steel vapor penetrated laterally into the pore network (Fig. 11). The thickness of the steel cover on Ti particles decreases with increasing distance from the side wall.

With time the steel layer thickness on the WI's increase and may connect with neighboring WI's to form ''wetted bridges'' and finally a 3D Ti-containing steel melt network will develop, which is connected with the top surface. The original steel melt can now use the existing melt network to infiltrate and fill the remaining empty pore space.

The observed penetration rates are not compatible with a Darcy's law type infiltration, which predicts a square root dependency between infiltration depth and time. The equality of the slopes between sample A100T40-20 and A20T40-20 implies that the rate determining process is independent of the pore radius. As rate limiting step to explain the linear infiltration rate observed for SiC preforms infiltrated by CoSi melts, melt spreading on preform grains was proposed.[31] The equation presented by the latter authors does indeed not depend on the pore radius. However, the proposed equation is biased and does not explain the linear infiltration behavior in the present system. For longer dwell times a linear dependence of melt drop radius spreading on time was observed.[33,34] The driving forces were described to be diffusion and dissolution processes at the triple line (metal-ceramic-vacuum) and give a possible explanation for the linear dependence of infiltration height on time. Additionally, it was shown in a previous study that a vacuum atmosphere is needed for a successful infiltration when using reactive metals as activator.[17]

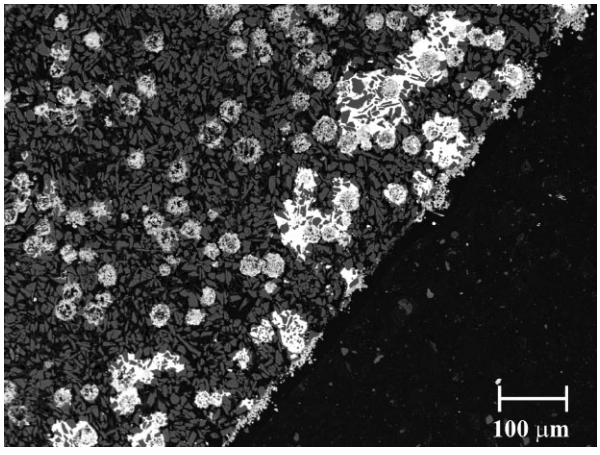

Fig. 11. Side wall of an A20T40-20 sample with WI's. A decrease in steel concentration with distance from the side wall is obvious. The adjacent bulk area is within Z3 of the sample.

The infiltration rate for short dwell times is difficult to interpret because of the shortage of data. For the A20T40-20 sample, a linear as well as a power law approach $t^{1/n}$ can be used to describe the infiltration depth versus time. However, the plotted data show an accelerated infiltration relative to the infiltration time. Considering the infiltration mechanism described above, such an offset is expected. Before the infiltration front can penetrate into the preform, WBs between the activator particles nearest to the surface have to be established. Considering the advanced penetration after 13 min in the A100T40 samples, this process must be very rapid.

According to the activated infiltration model presented above, infiltration will only occur when WB's between activator particles are established. The average distance between activator particles is thus the most critical parameter. The maximum surface to surface distance between nearest neighbor particles for which under the given conditions infiltration was observed, is between 20 and 30 μm[35] The latter value is the average next nearest neighbor distance for A100T40 samples with 3 wt% Ti, which did not infiltrate at all. This threshold range is consistent with the observation that none of the A100T200 samples were infiltrated, in which the nearest neighbor distance is above the threshold value (~25 μm) even for the sample with the highest activator content (20 wt%; 42 μm). The absence of infiltration in areas with low Ti particle concentration (s. Fig. 6) is also compatible with the proposed mechanism.

Conclusions

The activated infiltration experiments in the X3CrNi13-4 – alumina sample revealed a new activation mechanism. Metal transport through the gas phase and condensation on the activator particles have been shown to be the initial infiltration step. Liquid spreading along metal pathways is proposed as rate limiting step for infiltration. Parameters that in conventional infiltration scenario are of secondary importance, such as equilibrium gas pressure over the melt, supersaturation, activator distribution etc., play an important role for the infiltration performance of such activated system. Melt spreading driven by diffusion or dissolution processes at the triple line are possible reasons for the linear time dependent infiltration behavior. Additionally, in the ceramic-

steel system activated with reactive metals a vacuum atmosphere is needed for successful infiltration. This new insight allows a more straightforward selection of potential activators and to optimize preform microstructures for non-wetting ceramic-metal systems.

[1] D. B. Miracle, *Comp. Sci. Technol.* **2005**, *65*, 2526.
[2] A. Mattern, B. Huchler, D. Staudenecker, R. Oberacker, A. Nagel, M. J. Hoffmann, *J. Eur. Ceram. Soc.* **2004**, *24*, 3399.
[3] M. Rosso, *J. Mater. Proc. Technol.* **2006**, *175*, 364.
[4] D. J. Lloyd, *Int. Mater. Rev.* **1994**, *39*, 1.
[5] K. Lemster, U. E. Klotz, S. Fischer, P. Gasser, J. Kuebler, *Proc. Conf. Titan. Wiley VCH, Weinheim* **2003**, *10*, 2515.
[6] J. Kuebler, K. Lemster, P. Gasser, U. E. Klotz, T. Graule, presented at the *28th International Cocoa Beach Conference and Exposition on Advanced Ceramics and Composites*, Cocoa Beach **2004**, unpublished.
[7] K. Lemster, T. Graule, J. Kuebler, *Mater. Sci. Eng, A* **2005**, *393*, 229.
[8] K. Lemster, T. Graule, T. Minghetti, C. Schelle, J. Kuebler, *Mater. Sci. Eng, A* **2006**, *420*, 296.
[9] K. Lemster, M. Delporte, T. Graule, J. Kuebler, *Cer. Inter.* **2006**, *20*, 80.
[10] N. Froumin, M. Eisenstein, M. Polak, *Scripta Mat.* **1999**, *41*, 1205.
[11] R. Voytovych, L. Y. Ljungberg, N. Eustathopoulos, *Scripta Mat.* **1999**, *51*, 431.
[12] A. A. Amadeh, J. C. Labbe, P. E. Quintard, *J. Eur. Ceram. Soc.* **2005**, *25*, 101.
[13] C. A. Leon-Patino, R. A. L. Drew, *Curr. Opin. Solid State Mater. Sci.* **2005**, *9*, 211.
[14] N. Eustathopoulos, M. G. Nicholas, B. Drevet, *Wettability at High Temperatures - Pergamon Material Series*, Vol. 3(Ed: R. W. Cahn), Pergamon, Oxford **1999**, 229.
[15] F. Ortega-Celaya, M. I. Pech-Canul, J. Lopez-Cuevas, J. C. Rendon-Angeles, M. A. Pech-Canul, *J. Mater. Proc. Technol.* **2007**, *183*, 368.
[16] K. M. Shorowordi, T. Laoui, A. S. M. A. Haseeb, J. P. Celis, L. Froyen, *J. Mater. Proc. Technol.* **2003**, *142*, 738.
[17] Y. Kajikawa, T. Nukami, M. C. Flemings, *Metall. Mater. Trans. A* **1995**, *26(A)*, 2155.
[18] J.-G. Li, *Ceram. Int.* **1994**, *20*, 391.
[19] C. C. Lin, R. B. Chen, R. K. Shiue, *J. Mater. Sci.* **2001**, *36*, 2145.
[20] P. Kritsalis, V. Merlin, L. Coudurier, N. Eustathopoulos, *Acta Metall. Mater.* **1992**, *40*, 1167.
[21] A. Kar, S. Mandal, K. Venkateswarlu, A. K. Ray, *Mater. Charact.* **2007**, *58*, 555.
[22] A. Koltsov, M. Dumont, F. Hodaj, N. Eustathopoulos, *Mater. Sci. Eng, A* **2006**, *415*, 171.
[23] C. Englisch, *Doctoral Thesis*, EPF Lausanne, **1999**.
[24] G. Krauss, J. Kuebler, E. Trentini, *Mater. Sci. Eng, A* **2002**, *337*, 315.
[25] R. M. German, *MPIF Metal Powder Industries Federation*, Princeton **1989**.
[26] E. W. Washburn, *Am. Phys. Soc, 2nd Ser.* **1921**, *17*, 374.
[27] B. V. Zhmud, F. Tiberg, K. Hallstensson, *J. Colloid Interface Sci.* **2000**, *282*, 263.
[28] K. P. Plucknett, P. F. Becher, *J. Am. Ceram. Soc.* **2001**, *84*, 55.
[29] M. Rodriguez-Reyes, M. I. Pech-Canul, E. E. Parras-Medecigo, A. Gorokhovsky, *Mater. Lett.* **2003**, *57*, 2081.
[30] S. Fischer, unpubished *Diploma Thesis*, University of Fribourg, Fribourg **2003**.
[31] Y. Pan, X. S. Yi, *J. Am. Ceram. Soc.* **1990**, *82*, 3459.
[32] C. Toy, W. D. Scott, *J. Am. Ceram. Soc.* **1990**, *73*, 97.
[33] K. Landry, N. Eustathopoulos, *Acta Mater.* **1996**, *44*, 3923.
[34] N. Eustathopoulos, *Acta Mater.* **1998**, *46*, 319.
[35] S. Vasic, B. Grobety, J. Kuebler, T. Graule, L. Baumgartner, *J. Mater. Res.* **2007**, *22*, 1414.
[36] M. Humenik, W. D. Kingery, *J. Am. Ceram. Soc.* **1954**, *37*, 18.
[37] F. A. Halden, W. K. Kingery, *J. Phys. Chem.* **1955**, *59*, 557.
[38] K. Nogi, K. Ogino, *Can. Metall. Q.* **1983**, *22*, 19.
[39] E. Kapilashrami, A. Jakobsson, A. K. Lahiri, S. Seetharaman, *Metall. Mat. Trans. B.* **2003**, *34*, 193.
[40] R. Asthana, N. Sobczak, *JOM e-journal* (www.tms.org/pubs/journals/JOM/0001/Asthana/Asthana-0001.html), **2000**.
[41] N. Takiuchi, T. Taniguchi, Y. Tanaka, N. Shinozaki, K. Mukai, *J. Jpn. Inst. Met.* **1991**, *55*, 180.
[42] N. Kishimoto, T. Tanabe, H. Yoshida, R. Watanabe, *J. Nucl. Mater.* **1984**, *120*, 254.
[43] L. C. Zhong, M. Zeze, K. Mukai, *Acta Metal. Sin.* **2004**, *17*, 795.
[44] K. Mukai, L. Zhong, M. Zeze, *ISIJ Int.* **2006**, *46*, 1810.
[45] T. Suzuki, T. Koseki, *Tetsu-to-Hagané* **2006**, *92*, 411.
[46] K. Mukai, Z. S. Li, M. Zeze, *Mater. Trans.* **2002**, *43*, 1724.
[47] A. I. Zaitsev, N. E. Shelkova, A. D. Litvina, E. K. Shakhpazov, B. M. Mogutnov, *High Temp.* **2001**, *39*, 388.
[48] C. B. Alcock, *CRC Handbook of chemistry and physics*, 84th edn. (Ed: D. R. Lide), CRC Press LLC, London **2004**, *134(4)*.